Water-unlocked formation of active oxygen vacancies in perovskite fuel-cell cathodes

Desheng Feng,[1,2,#] Tianjiu Zhu,[1,#] Hengyue Xu,[3,#] Vanessa K Peterson,[4*] Anita D'Angelo,[5] Penghui Yan,[1] Xiaoyang Du,[2] Xiaohe Tian,[2] Dan Li[2,6], Zhonghua Zhu[1*], Mengran Li,[2*]

1. School of Chemical Engineering, The University of Queensland, Brisbane, 4072, Australia
2. Department of Chemical Engineering, the University of Melbourne, Melbourne, 3010, Australia
3. Tsinghua Shenzhen International Graduate School, Tsinghua University, Shenzhen, 518055, P.R. China
4. Australian Centre for Neutron Scattering, Australian Nuclear Science and Technology Organisation, Sydney, New South Wales, Australia
5. Australian Synchrotron, Australian Nuclear Science and Technology Organization, Clayton, Victoria, 3168 Australia
6. Department of Chemical and Biological Engineering, The Hong Kong University of Science and Technology, Hong Kong, 999077 China

# These authors contributed equally: Desheng Feng, Tianjiu Zhu, Hengyue Xu
Corresponding authors:
V. K. Peterson: vanessa.peterson@ansto.gov.au
Z. Zhu: z.zhu@uq.edu.au
M. Li: aaron.li1@unimelb.edu.au

Methods

Material synthesis

Cathode materials used in this study were synthesised using a conventional sol–gel method. Taking BCFZY as an example, stoichiometric amounts of $Ba(NO_3)_2$ (99%, Sigma-Aldrich), $Co(NO_3)_2 \cdot 6H_2O$ (98%, Sigma-Aldrich), $Fe(NO_3)_3 \cdot 9H_2O$ (98%, Sigma-Aldrich), $ZrO(NO_3)_2 \cdot xH2O$ (99%, Sigma-Aldrich), and $Y(NO_3)_3 \cdot 6H2O$ (99%, Sigma-Aldrich) were dissolved in deionised water. Citric acid (CA, 99.5%, Sigma-Aldrich) was then added to the solution, followed by ethylenediaminetetraacetic acid (EDTA, 99%, Sigma-Aldrich) dissolved in 28% ammonia solution (Westlab). The molar ratio of total metal cations:CA:EDTA was maintained at 2:3:3. Ammonia solution was subsequently added to adjust the pH to ~10. The solution was heated on a hot plate at 80 °C to evaporate water until a gel formed. The gel was then dried in an oven at 260 °C to obtain ash, which was calcined at 1000 °C for 5 h in a Labec BF 08/14 muffle furnace to obtain the final cathode material.

Lab X-ray powder diffraction

X-ray powder diffraction (XRD) measurements were conducted at the Centre for Microscopy and Microanalysis (CMM), The University of Queensland, using a Bruker D8 Advance diffractometer. Instrumental parameters were determined using the National Institute of Standards and Technology (NIST) silicon 640c[1] standard reference material (SRM) through Rietveld refinement in GSAS-II[2].

Synchrotron X-ray powder diffraction

Synchrotron X-ray powder diffraction (SXRD) data were collected at the Australian Synchrotron, Australian Nuclear Science and Technology Organisation (ANSTO). The samples were first mixed with quartz powder at a 50 wt.% ratio and then loaded into quartz capillaries with a diameter of 0.7 mm. SXRD patterns were collected under ambient conditions before

conducting the high-temperature measurements. For high-temperature SXRD measurements, samples were loaded into 0.7 mm glass capillaries and heated using a Cyberstar hot gas blower at a rate of 6 °C min^{-1}. Dry and humid air were supplied to the sample using an XCS gas delivery system. Instrumental parameters were determined using the NIST $La^{11}B_6$ 660b SRM through Rietveld refinement in GSAS-II.

Neutron powder diffraction

Neutron powder diffraction (NPD) data were collected using the high-intensity diffractometer Wombat at the Australian Centre for Neutron Scattering (ACNS), ANSTO.[3] Before heating, room-temperature NPD patterns were collected under ambient conditions with the samples loaded in quartz tubes inside the furnace. For the high-temperature NPD measurements, the samples were then heated in an ILL-type vacuum furnace equipped with a niobium element at a rate of 6 °C min^{-1}. After reaching 600 °C, the sample was held at 600 °C for 30 min before cooling passively (Figs. S25 and S26). The contribution of the furnace to the NPD pattern is shown in Fig. S27. Instrumental parameters were determined using the NIST $La^{11}B_6$ 660b SRM[4] through Rietveld refinement in GSAS-II.

Refinement of room temperature SXRD and NPD results

The compositions of BCFZY and BCFZYYb were determined by joint refinement of SXRD and NPD data measured at room temperature. The Rietveld refinements were performed using GSAS-II[2]. Instrument profile parameters for SXRD and NPD were first determined from NIST standard reference materials SRM 660b[4] and subsequently fixed during the refinement of the sample data. The background was modelled using Chebyshev polynomials with 30 coefficients for NPD data and 20 coefficients for SXRD data. Sample displacement parameters (along-beam and across-beam offsets) were refined at the beginning of the refinement.

Both BCFZY and BCFZYYb were modelled using two major cubic phases (space group $Pm\bar{3}m$) with an initial structural model based on $BaZr_{0.5}Fe_{0.5}O_3$.[5] The refinement was initiated using the nominal compositions with fixed site occupancies. Because Zr and Y have similar atomic numbers and neutron scattering lengths,[6] they are treated identically in the refinement. The lattice parameters and phase fractions of the two phases were first refined. These parameters were then fixed while the site occupancies were refined to minimise correlations between occupancy and lattice parameters. The occupancies of equivalent sites in the two phases were constrained to be identical, and the isotropic displacement parameters (U_{iso}) were constrained in the same manner.

The U_{iso} values were first refined for all atomic species. Subsequently, the occupancies of Ba, O and the *B*-site cations were refined individually while their corresponding U_{iso} values were refined simultaneously. After convergence, the occupancies of all atomic species were refined together with the U_{iso} values. Finally, the lattice parameters and phase fractions were released, and all parameters were refined simultaneously until convergence. The microstrain parameter was initially fixed at 1000 and was only released for refinement after convergence of the structural and profile parameters to minimise parameter correlations.

High temperature NPD refinement

Temperature-dependent oxygen non-stoichiometry was determined by sequential refinement of the NPD data collected at elevated temperatures. The refined structural model obtained from the room-temperature NPD refinement served as the starting point for the sequential refinement, which was performed from low to high temperatures. The sample displacement parameter and cation occupancies were fixed at the values obtained from the room-temperature refinement, as they were not expected to vary with temperature. The lattice parameter, microstrain, oxygen occupancy, U_{iso}, and background coefficients were refined for each dataset.

X-ray adsorption spectroscopy (XAS)

X-ray absorption spectroscopy data were collected at the MEX-1 beamline at the Australian Synchrotron, ANSTO. The as-synthesised cathode powders were mixed with cellulose and pelletised. The pellets were then used to measure the Co and Fe K-edge absorption spectra in both transmission and fluorescence modes. As shown in Figs. S28 and S29, Yb doping has a negligible impact on the Co and Fe local environments under dry conditions.

Computational details

All spin-polarised density functional theory (DFT) calculations were performed using the Vienna *Ab initio* Simulation Package (VASP).[7] The projector augmented wave (PAW) method was employed to describe the electron–ion interactions.[8] The exchange–correlation effects were treated within the generalised gradient approximation (GGA) using the Perdew–Burke–Ernzerhof (PBE) functional.[9] The ionic structures were fully relaxed using the conjugate-gradient algorithm until the residual Hellmann–Feynman forces on each atom were below 0.03 eV $Å^{-1}$. The electronic self-consistency loop was converged to 1×10^{-5} eV, using a Gaussian smearing of 0.05 eV[10,11] and an energy cutoff of 500 eV.[12,13] Brillouin-zone sampling was carried out using a Γ-centered Monkhorst–Pack grid of 3×3×3 k-points. For structural optimisation, surface models included a 15 Å vacuum layer to eliminate spurious interactions between periodic images, and the lower half of the slab was fixed to mimic bulk conditions.[14–16] Long-range dispersion interactions were included *via* the DFT-D3 method with Becke–Johnson damping. Strong on-site Coulomb interactions were treated within the Dudarev formulation of DFT+U, with U_{eff}= 3.3 eV applied to the Co 3d states.[17,18]

Oxygen-vacancy formation energy

The oxygen-vacancy formation energy was evaluated using an O_2 reference according to:[18]

$$E_{\mathrm{f}}(V_{\mathrm{O}}) = E_{\mathrm{def}} + \frac{1}{2}E_{\mathrm{O_2}} - E_{\mathrm{pristine}}$$

where E_{pristine} and E_{def} are the total energies of the stoichiometric and oxygen-deficient structures, respectively, and $E_{\mathrm{O_2}}$ is the total energy of an isolated O_2 molecule computed consistently at the same DFT level.

Neutron spectroscopy

Neutron spectroscopy measurements were conducted using the Time-of-Flight Spectrometer Pelican at ACNS, ANSTO.[19,20] A vanadium can was measured to obtain the instrumental resolution function of Pelican (Fig. S30). The neutron wavelength used in this study was 6 Å. Before neutron spectroscopy measurements, samples were hydrated at 400 °C in 10 vol.% humid N_2 for 12 h. The pre-hydrated samples were then sealed in quartz ampoules (Fig. S31) and loaded into Pelican. Figs. S32 and Fig. S33 show the S(Q) profiles, where the (100) reflection of the cathode materials was identified to ensure proper sample alignment. Samples were heated using a vacuum furnace at a ramping rate of 5 °C min^{-1}. After reaching each target temperature (500, 600, and 700 °C), data were collected for 8 h before heading to the next temperature. Following completion of all measurements, the samples were cooled to room temperature, and water droplets were observed on the inner wall of the quartz ampoule (Fig. S34), confirming the presence of water released during heating. After the measurements, the samples were removed from the ampoules, and neutron spectroscopy data of the empty quartz ampoules were collected for background subtraction (Fig. S35).

Water uptake measurement

The water uptake of the samples was measured using a PerkinElmer TGA 4000 thermogravimetric analyser. Approximately 200 mg of sample was loaded into an alumina crucible and heated to 400 °C. The samples were equilibrated in flowing dry N_2 at 400 °C for at least 10 h before switching to humidified N_2. The hydration content was determined from the mass change between the dry and humid conditions.

H_2O-TPD-MS

H_2O-TPD-MS measurements were performed using BELCAT and BELMass systems. Approximately 0.1 g of powder was first pre-hydrated in 10 vol.% humidified N_2 at 400 °C for 10 h. The pre-hydrated sample was then loaded into a U-shaped quartz tube for TPD analysis. During the measurement, samples were heated to 800 °C at a ramping rate of 2 °C min^{-1} under flowing Ar. The desorbed gases released during heating were continuously monitored using the BELMass mass spectrometry.

Electrical conductivity relaxation (ECR)

Powder samples were first pressed into rectangular bars and sintered at 1100 °C to obtain dense specimens. The electrical conductivity of the materials was measured using a four-probe method in dry air (Fig. S36) over the temperature range of 300–700 °C. For humidity-dependent measurements, the samples were stabilised at 500 °C in dry air for more than 10 h. Humidified air was subsequently introduced while continuously monitoring the evolution of electrical conductivity for more than 30 min.

Symmetric and Single-Cell Fabrication

For symmetric cell fabrication, electrolyte powders (SDC and BZCYYb) were first dry-pressed into pellets and sintered at 1450 °C for 5 h in a Labec BF 08/14 muffle furnace to obtain dense electrolyte disks. Cathode inks were prepared by mixing 5 g cathode powders with 45 mL of isopropanol and 5 mL of glycerol using a Planetary Mill PULVERISETTE 5/2. The inks were subsequently spray-coated onto both sides of the electrolyte disks and sintered at 950 °C for 2 h in a Labec BF 08/14 muffle furnace.

For anode-supported single-cell fabrication, anode (60 wt.% NiO and 40 wt.% BZCYYb) and electrolyte powders were co-pressed to form half-cells, which were then sintered at 1450 °C for 5 h in a Labec BF 08/14 muffle furnace to densify the electrolyte layer. Cathode inks were

spray-coated onto the electrolyte surface and subsequently sintered at 950 °C for 2 h in a Labec BF 08/14 muffle furnace.

Electrochemical Characterisation

Electrochemical impedance spectroscopy (EIS) measurements were performed using an Autolab PGSTAT302N Metrohm potentiostat to evaluate cell resistance. The open-circuit voltage (OCV) of each cell was first measured, followed by the application of a 10 mV sinusoidal perturbation over a frequency range from 10^6 to 0.01 Hz.

Linear sweep voltammetry (LSV) was conducted to evaluate single-cell performance. The OCV was first measured using a four-probe configuration, after which the cell voltage was swept to 0.2 V at a scan rate of 0.1 V s^{-1} while recording the current response.

Chronoamperometry measurements were performed to evaluate cell durability by applying a constant current to the cell while continuously recording the cell voltage every 10 min.

Supplementary Tables

Supplementary Table 1 SXRD and NPD joint refinement of BCFZY at room temperature

Atom	Site Multiplicity	*x*	*y*	*z*	Occupancy	Uiso (Å^2)
BCFZY-1, a = 4.11698(3) Å, weight fraction,[a] 54.5(5)%, $Pm\bar{3}m$						
Ba	1	0.5	0.5	0.5	0.97(5)	0.0269(7)
Zr/Y[b]	1	0	0	0	0.2(1)	0.0348(9)[c]
Fe	1	0	0	0	0.42(4)	0.0348(9)[c]
Co	1	0	0	0	0.3(1)	0.0348(9)[c]
O	3	0.5	0	0	0.86(4)	0.0381(8)
BCFZY-2, a = 4.11289(4) Å, weight fraction [a] 45.5(5)%, $Pm\bar{3}m$						
Ba	1	0.5	0.5	0.5	0.97(5)	0.0269(7)
Zr/Y[b]	1	0	0	0	0.2(1)	0.0348(9)[c]
Fe	1	0	0	0	0.42(4)	0.0348(9)[c]
Co	1	0	0	0	0.3(1)	0.0348(9)[c]
O	3	0.5	0	0	0.86(4)	0.0381(8)
Goodness of fit (GOF) = 3.41						
Weighted profile R-factor (wR) = 6.43%						

[a] Data indicated a main phase of BCFZY with a distribution of lattice parameters that could not be fully resolved in the data and were modelled reasonably well using two $Pm\bar{3}m$ phases with all parameters of these phases constrained to be the same, except for the lattice constant.
[b] Zr and Y are indistinguishable and combined.
[c] Atomic displacement parameters are constrained to be equal for atoms at the same site.

Supplementary Table 2 SXRD and NPD joint refinement of BCFZYYb at room temperature

Atom	Site Multiplicity	*x*	*y*	*z*	Occupancy	Uiso (Å^2)
BCFZYYb-1, a = 4.11912(4) Å, weight fraction 41.3(3)%,[a] $Pm\bar{3}m$						
Ba	1	0.5	0.5	0.5	1.03(1)	0.0317(8)
Zr/Y[b]	1	0	0	0	0.2(2)	0.0395(8)[c]
Yb	1	0	0	0	0.05(4)	0.0395(8)[c]
Co	1	0	0	0	0.37(8)	0.0395(8)[c]
Fe	1	0	0	0	0.42(6)	0.0395(8)[c]
O	3	0.5	0	0	0.835(8)	0.0381(8)
BCFZYYb-2, a = 4.12302(3) Å, weight fraction 58.7(3)%,[a] $Pm\bar{3}m$						
Ba	1	0.5	0.5	0.5	1.03(1)	0.0317(8)
Zr/Y[b]	1	0	0	0	0.2(2)	0.0395(8)[c]
Yb	1	0	0	0	0.05(4)	0.0395(8)[c]
Co	1	0	0	0	0.37(8)	0.0395(8)[c]
Fe	1	0	0	0	0.42(6)	0.0395(8)[c]
O	3	0.5	0	0	0.835(8)	0.0381(8)
Goodness of fit (GOF) = 3.72						
Weighted profile R-factor (wR) = 2.95%						

[a] Data indicated a main phase of BCFZYYb with a distribution of lattice parameters that could not be fully resolved in the data and were modelled reasonably well using two $Pm\bar{3}m$ phases with all parameters of these phases constrained to be the same, except for the lattice constant.

[b] Zr and Y are indistinguishable and combined.

[c] Atomic displacement parameters are constrained to be equal for atoms at the same site.

Supplementary Table 3 NPD refinement of BCFZY in dry air between 450 and 600 °C

Temperature (°C)	Rwp (%)	GOF	Lattice parameter (Å)	esd	Oxygen occupancy	esd
451	1.91	11.57	4.203	0.003	0.791	0.003
453	1.94	11.64	4.207	0.003	0.773	0.003
455	1.92	11.65	4.198	0.003	0.781	0.003
458	1.88	11.42	4.203	0.004	0.785	0.003
460	1.89	11.48	4.202	0.004	0.782	0.003
462	1.96	11.83	4.206	0.004	0.784	0.003
464	1.90	11.49	4.206	0.003	0.779	0.003
466	1.94	11.81	4.201	0.003	0.773	0.003
468	1.81	10.95	4.202	0.003	0.788	0.003
471	1.94	11.78	4.202	0.004	0.787	0.003
473	1.96	11.91	4.198	0.004	0.786	0.003
475	1.92	11.74	4.201	0.004	0.778	0.003
477	1.93	11.71	4.205	0.004	0.785	0.003
479	1.98	11.95	4.204	0.004	0.785	0.003
481	1.93	11.72	4.205	0.003	0.771	0.003
483	1.91	11.49	4.207	0.003	0.778	0.003
485	1.94	11.75	4.200	0.004	0.778	0.003
488	1.86	11.26	4.203	0.003	0.780	0.003
490	1.94	11.69	4.206	0.004	0.784	0.003
492	2.01	12.19	4.201	0.004	0.788	0.003
494	1.92	11.76	4.200	0.003	0.777	0.003
496	1.87	11.39	4.203	0.003	0.770	0.003
498	1.87	11.41	4.204	0.004	0.782	0.003
500	1.95	11.8	4.206	0.004	0.782	0.003
502	1.93	11.69	4.201	0.004	0.776	0.003
505	1.93	11.72	4.210	0.003	0.780	0.003
507	1.89	11.45	4.205	0.003	0.777	0.003
509	1.96	11.9	4.207	0.005	0.784	0.003
511	1.89	11.49	4.201	0.004	0.781	0.003
513	1.77	10.75	4.203	0.004	0.777	0.002
515	1.87	11.38	4.198	0.004	0.777	0.003
518	1.93	11.77	4.206	0.004	0.774	0.003
520	1.96	11.9	4.198	0.004	0.787	0.003
522	1.95	11.81	4.209	0.004	0.787	0.003
524	1.83	11.13	4.207	0.003	0.775	0.003
526	1.89	11.43	4.205	0.004	0.772	0.003
528	2.00	12.16	4.209	0.004	0.785	0.003
530	1.91	11.65	4.203	0.003	0.778	0.003
533	1.85	11.24	4.202	0.003	0.777	0.003
535	1.97	11.97	4.206	0.003	0.776	0.003
537	1.84	11.26	4.207	0.004	0.776	0.003
539	1.83	11.15	4.199	0.004	0.778	0.003

541	1.87	11.28	4.206	0.004	0.776	0.003
543	1.94	11.69	4.211	0.006	0.775	0.003
546	1.83	11.17	4.206	0.004	0.774	0.003
548	1.88	11.4	4.204	0.004	0.770	0.003
550	1.89	11.48	4.200	0.003	0.791	0.003
552	1.96	12	4.207	0.004	0.781	0.003
554	1.86	11.33	4.205	0.003	0.777	0.003
556	1.87	11.39	4.209	0.004	0.780	0.003
558	1.91	11.56	4.199	0.004	0.778	0.003
561	1.90	11.6	4.203	0.004	0.780	0.003
563	1.85	11.2	4.205	0.004	0.773	0.003
565	1.88	11.38	4.208	0.004	0.763	0.003
567	1.88	11.37	4.208	0.004	0.781	0.003
569	1.87	11.34	4.207	0.004	0.773	0.003
571	1.87	11.39	4.199	0.004	0.786	0.003
574	1.90	11.43	4.206	0.003	0.773	0.003
576	1.87	11.29	4.206	0.004	0.771	0.003
578	1.89	11.42	4.207	0.003	0.787	0.003
580	1.88	11.48	4.213	0.005	0.781	0.003
582	1.87	11.36	4.205	0.004	0.782	0.003
584	1.76	10.69	4.200	0.003	0.782	0.003
586	1.87	11.31	4.212	0.004	0.762	0.003
588	1.89	11.56	4.211	0.004	0.783	0.003
591	1.87	11.36	4.211	0.004	0.778	0.003
593	1.86	11.34	4.207	0.004	0.778	0.003
595	1.87	11.4	4.208	0.004	0.775	0.003
597	1.88	11.43	4.208	0.004	0.788	0.003
599	1.88	11.46	4.211	0.004	0.775	0.003
600	1.86	11.3	4.203	0.003	0.775	0.003

Supplementary Table 4 NPD refinement of BCFZY in 3 vol.% D_2O air between 450 and 600 °C

Temperature (°C)	Rwp (%)	GOF	Lattice parameter (Å)	esd	Oxygen occupancy	esd
450	1.79	11.21	4.203	0.003	0.793	0.002
453	1.70	10.64	4.207	0.003	0.776	0.002
455	1.86	11.67	4.198	0.003	0.792	0.003
457	1.76	11.07	4.203	0.004	0.781	0.002
459	1.77	11.09	4.202	0.004	0.792	0.002
461	1.84	11.49	4.206	0.004	0.793	0.003
463	1.81	11.44	4.206	0.003	0.780	0.002
465	1.79	11.18	4.201	0.003	0.803	0.003
468	1.79	11.15	4.202	0.003	0.784	0.002
470	1.76	11.03	4.202	0.004	0.794	0.002
472	1.84	11.65	4.198	0.004	0.789	0.003
474	1.75	10.96	4.201	0.004	0.787	0.002
476	1.76	11.02	4.205	0.004	0.793	0.002
478	1.73	10.90	4.204	0.004	0.791	0.002
480	1.79	11.16	4.205	0.003	0.795	0.003
482	1.80	11.28	4.207	0.003	0.796	0.003
485	1.79	11.30	4.200	0.004	0.775	0.002
487	1.82	11.37	4.203	0.003	0.789	0.003
489	1.83	11.49	4.206	0.004	0.783	0.003
491	1.75	10.92	4.201	0.004	0.795	0.003
493	1.83	11.52	4.200	0.003	0.782	0.003
495	1.87	11.81	4.203	0.003	0.779	0.003
497	1.79	11.28	4.204	0.004	0.784	0.003
500	1.73	10.80	4.206	0.004	0.794	0.002
502	1.85	11.61	4.201	0.004	0.794	0.003
504	1.77	11.16	4.210	0.003	0.773	0.002
506	1.75	11.08	4.205	0.003	0.782	0.002
508	1.72	10.79	4.207	0.005	0.775	0.002
510	1.82	11.31	4.201	0.004	0.788	0.003
513	1.83	11.47	4.203	0.004	0.795	0.003
515	1.80	11.34	4.198	0.004	0.791	0.003
517	1.76	11.04	4.206	0.004	0.795	0.003
519	1.74	10.82	4.198	0.004	0.780	0.002
521	1.77	11.15	4.209	0.004	0.792	0.003
523	1.81	11.35	4.207	0.003	0.777	0.003
525	1.81	11.32	4.205	0.004	0.786	0.003
527	1.71	10.78	4.209	0.004	0.784	0.002
530	1.79	11.28	4.203	0.003	0.774	0.003
532	1.84	11.47	4.202	0.003	0.778	0.003
534	1.80	11.36	4.206	0.003	0.786	0.003
536	1.75	11.05	4.207	0.004	0.781	0.003
538	1.75	11.00	4.199	0.004	0.778	0.003

541	1.70	10.63	4.206	0.004	0.773	0.002
542	1.75	10.94	4.211	0.006	0.787	0.003
545	1.75	10.97	4.206	0.004	0.772	0.002
547	1.72	10.71	4.204	0.004	0.785	0.002
549	1.74	10.86	4.200	0.003	0.776	0.003
551	1.71	10.74	4.207	0.004	0.771	0.002
553	1.77	11.10	4.205	0.003	0.780	0.003
556	1.70	10.71	4.209	0.004	0.784	0.003
558	1.84	11.53	4.199	0.004	0.771	0.003
560	1.79	11.22	4.203	0.004	0.784	0.003
562	1.83	11.54	4.205	0.004	0.791	0.003
564	1.76	11.16	4.208	0.004	0.784	0.003
566	1.67	10.51	4.208	0.004	0.784	0.002
568	1.79	11.29	4.207	0.004	0.779	0.003
571	1.81	11.34	4.199	0.004	0.773	0.003
573	1.84	11.42	4.206	0.003	0.775	0.003
575	1.76	11.06	4.206	0.004	0.784	0.003
577	1.78	11.20	4.207	0.003	0.762	0.003
579	1.82	11.46	4.213	0.005	0.786	0.003
581	1.72	10.78	4.205	0.004	0.774	0.003
583	1.70	10.80	4.200	0.003	0.775	0.002
586	1.72	10.82	4.212	0.004	0.773	0.003
588	1.73	10.83	4.211	0.004	0.788	0.003
590	1.69	10.69	4.211	0.004	0.768	0.002
592	1.73	10.84	4.207	0.004	0.774	0.003
594	1.71	10.76	4.208	0.004	0.783	0.003
596	1.72	10.66	4.208	0.004	0.783	0.003
599	1.77	11.05	4.211	0.004	0.774	0.003
600	1.72	10.77	4.203	0.003	0.773	0.003

Supplementary Table 5 NPD refinement of BCFZYYb in dry air between 450 and 600 °C

Temperature (°C)	Rwp (%)	GOF	Lattice parameter (Å)	esd	Oxygen occupancy	esd
450	1.99	11.98	4.198	0.002	0.772	0.002
452	1.98	12.00	4.200	0.002	0.789	0.002
455	2.00	12.08	4.199	0.002	0.777	0.002
457	1.95	11.85	4.199	0.002	0.782	0.002
459	2.02	12.20	4.198	0.002	0.784	0.002
461	1.98	11.97	4.202	0.002	0.783	0.002
463	2.05	12.38	4.195	0.002	0.783	0.002
465	1.99	11.96	4.200	0.002	0.778	0.002
468	1.92	11.56	4.202	0.002	0.785	0.002
470	2.00	12.02	4.200	0.002	0.783	0.002
472	2.00	12.03	4.199	0.002	0.781	0.002
474	2.02	12.18	4.199	0.002	0.783	0.002
476	1.92	11.52	4.200	0.002	0.778	0.002
478	1.97	11.80	4.197	0.002	0.781	0.002
480	1.96	11.82	4.198	0.002	0.780	0.002
483	1.99	12.00	4.201	0.002	0.783	0.002
485	1.98	11.98	4.202	0.002	0.786	0.002
487	1.94	11.70	4.198	0.002	0.769	0.002
489	1.94	11.73	4.200	0.003	0.790	0.002
491	1.94	11.64	4.199	0.002	0.783	0.002
493	1.92	11.54	4.202	0.002	0.775	0.002
495	2.01	12.06	4.202	0.002	0.784	0.002
497	2.02	12.08	4.201	0.002	0.786	0.002
500	1.87	11.22	4.202	0.002	0.778	0.002
502	1.96	11.74	4.201	0.002	0.780	0.002
504	2.00	12.04	4.200	0.002	0.789	0.002
506	2.01	12.17	4.203	0.002	0.779	0.002
508	1.95	11.72	4.199	0.002	0.775	0.002
510	1.99	11.96	4.200	0.002	0.789	0.002
513	1.99	11.98	4.202	0.002	0.784	0.002
515	1.97	11.90	4.203	0.002	0.782	0.002
517	1.99	12.03	4.203	0.002	0.778	0.002
519	1.99	12.01	4.200	0.002	0.780	0.002
521	1.89	11.23	4.199	0.002	0.787	0.002
523	1.94	11.73	4.196	0.002	0.773	0.002
525	1.97	11.79	4.203	0.002	0.780	0.002
528	1.96	11.80	4.203	0.002	0.784	0.002
530	1.93	11.75	4.205	0.002	0.784	0.002
532	1.96	11.81	4.200	0.003	0.782	0.002
534	1.90	11.51	4.204	0.002	0.787	0.002
536	1.98	11.85	4.203	0.002	0.784	0.002
538	1.93	11.66	4.203	0.002	0.772	0.002

540	1.84	11.15	4.205	0.002	0.776	0.002
543	1.89	11.43	4.202	0.002	0.768	0.002
545	1.96	11.86	4.202	0.002	0.781	0.002
547	1.84	11.11	4.202	0.002	0.763	0.002
549	1.87	11.29	4.200	0.002	0.777	0.002
551	1.96	11.72	4.204	0.002	0.782	0.002
553	1.92	11.57	4.205	0.002	0.780	0.002
555	1.96	11.79	4.204	0.002	0.770	0.002
558	1.99	11.98	4.204	0.002	0.779	0.003
560	2.04	12.26	4.201	0.002	0.779	0.002
562	1.92	11.61	4.203	0.002	0.778	0.003
564	1.98	11.92	4.204	0.002	0.775	0.002
566	1.85	11.26	4.207	0.001	0.776	0.002
568	1.93	11.61	4.204	0.002	0.782	0.002
571	1.92	11.66	4.204	0.002	0.781	0.002
573	1.83	10.92	4.202	0.002	0.774	0.002
575	1.96	11.85	4.205	0.002	0.773	0.002
577	1.90	11.43	4.202	0.002	0.780	0.002
579	1.91	11.48	4.206	0.002	0.769	0.002
581	1.93	11.57	4.204	0.002	0.780	0.002
583	1.93	11.71	4.203	0.002	0.772	0.002
586	1.87	11.19	4.202	0.002	0.768	0.002
588	1.92	11.54	4.203	0.002	0.778	0.002
590	1.86	11.21	4.199	0.002	0.773	0.002
592	1.86	11.21	4.203	0.002	0.780	0.002
594	1.87	11.33	4.206	0.002	0.771	0.002
596	1.91	11.50	4.202	0.002	0.771	0.003
598	1.84	11.10	4.200	0.003	0.784	0.002
600	1.87	11.23	4.205	0.002	0.780	0.003

Supplementary Table 6 NPD refinement of BCFZYYb in 3 vol.% D_2O air between 450 and 600 °C

Temperature (°C)	Rwp (%)	GOF	Lattice parameter (Å)	esd	Oxygen occupancy	esd
451	1.91	11.85	4.199	0.002	0.779	0.003
453	1.93	12.10	4.198	0.002	0.783	0.003
455	1.94	12.11	4.195	0.002	0.783	0.002
458	1.90	11.92	4.196	0.002	0.779	0.002
460	1.91	11.78	4.200	0.002	0.777	0.002
462	1.96	12.19	4.197	0.002	0.788	0.002
464	1.95	12.15	4.195	0.002	0.778	0.002
466	1.91	12.04	4.199	0.002	0.776	0.003
468	1.97	12.35	4.201	0.002	0.786	0.003
470	1.89	11.93	4.196	0.003	0.782	0.002
473	1.96	12.16	4.200	0.002	0.778	0.003
475	1.98	12.43	4.202	0.002	0.783	0.002
477	1.98	12.40	4.199	0.002	0.785	0.003
479	2.00	12.48	4.197	0.002	0.790	0.003
481	1.97	12.36	4.197	0.002	0.788	0.003
483	1.90	11.91	4.196	0.002	0.783	0.003
485	1.97	12.30	4.195	0.002	0.772	0.003
488	2.01	12.45	4.196	0.002	0.786	0.002
490	1.96	12.32	4.200	0.002	0.773	0.003
492	1.88	11.73	4.200	0.002	0.775	0.003
494	1.95	12.09	4.198	0.002	0.786	0.003
496	1.98	12.36	4.198	0.002	0.772	0.002
498	1.90	11.91	4.198	0.003	0.792	0.003
500	1.99	12.53	4.199	0.002	0.774	0.003
502	2.01	12.48	4.201	0.002	0.775	0.002
505	1.89	11.74	4.200	0.002	0.785	0.003
507	1.94	12.07	4.199	0.002	0.782	0.003
509	2.00	12.52	4.200	0.002	0.781	0.003
511	1.87	11.64	4.202	0.002	0.781	0.003
513	1.92	12.06	4.199	0.002	0.779	0.003
515	1.93	11.94	4.202	0.002	0.777	0.002
518	1.91	11.93	4.199	0.002	0.773	0.003
520	1.89	11.81	4.194	0.003	0.785	0.003
522	1.93	12.01	4.200	0.002	0.780	0.003
524	1.86	11.55	4.202	0.002	0.780	0.003
526	1.81	11.27	4.197	0.002	0.778	0.003
528	1.95	12.15	4.202	0.002	0.780	0.002
530	1.88	11.70	4.199	0.002	0.774	0.002
533	1.88	11.70	4.201	0.002	0.781	0.003
535	1.94	12.17	4.202	0.001	0.782	0.003
537	1.89	11.82	4.201	0.002	0.774	0.003

539	1.90	11.76	4.200	0.002	0.780	0.003
541	1.86	11.62	4.202	0.002	0.764	0.003
543	1.87	11.73	4.199	0.002	0.771	0.003
546	1.92	12.04	4.203	0.002	0.772	0.002
548	1.95	12.07	4.200	0.003	0.772	0.003
550	1.86	11.66	4.200	0.002	0.782	0.003
552	1.92	12.00	4.200	0.002	0.782	0.003
554	1.90	11.86	4.203	0.002	0.766	0.003
556	1.92	12.03	4.202	0.002	0.774	0.003
558	1.91	11.91	4.202	0.002	0.779	0.003
561	1.89	11.83	4.204	0.002	0.783	0.003
563	1.93	12.11	4.203	0.002	0.777	0.003
565	1.86	11.65	4.204	0.002	0.766	0.003
567	1.88	11.86	4.204	0.002	0.781	0.003
569	1.83	11.39	4.201	0.002	0.767	0.003
571	1.82	11.34	4.202	0.002	0.784	0.003
573	1.87	11.72	4.204	0.002	0.764	0.003
576	1.82	11.38	4.202	0.002	0.772	0.002
578	1.80	11.18	4.204	0.002	0.769	0.003
580	1.78	11.15	4.201	0.002	0.775	0.003
582	1.89	11.75	4.204	0.002	0.759	0.002
584	1.86	11.56	4.201	0.002	0.775	0.002
586	1.86	11.56	4.204	0.002	0.777	0.003
589	1.89	11.81	4.205	0.002	0.785	0.003
591	1.87	11.70	4.203	0.002	0.783	0.003
593	1.86	11.66	4.203	0.002	0.769	0.003
595	1.78	11.20	4.203	0.002	0.767	0.002
597	1.85	11.59	4.203	0.002	0.770	0.003
599	1.86	11.61	4.205	0.002	0.766	0.003
600	1.89	11.81	4.204	0.002	0.770	0.003

Supplementary Table 7 ASR of BCFZYYb against reported single-phase perovskite oxides at 600 °C on a proton-conducting symmetric cell in humid air

Cathode	ASR @ 550 °C (Ω cm^2)	Reference
BCFZYYb	0.31	This study
BCFZY	0.52	This study
D-BFZ	0.50	[21]
GCCCO	0.50	[22]
BCFZYN	0.42	[23]
BCFNS	0.55	[24]
BCFZY-Mg	0.26	[25]
BCT	0.39	[26]
BCFZY7111	0.35	[27]
BCZYZICM	0.35	[28]
PBSCF	1.9	[29]
BSCF	1.27	[23]

Supplementary Figures

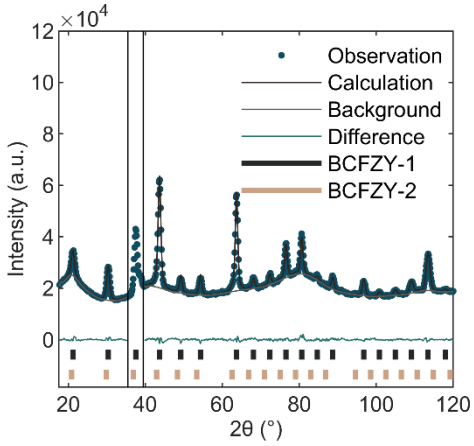

Supplementary Figure 1 NPD pattern of BCFZY at room temperature

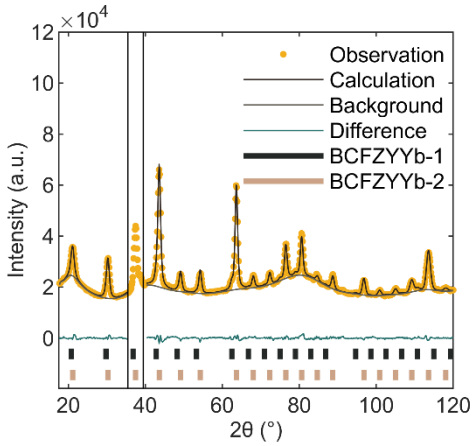

Supplementary Figure 2 NPD pattern of BCFZYYb at room temperature

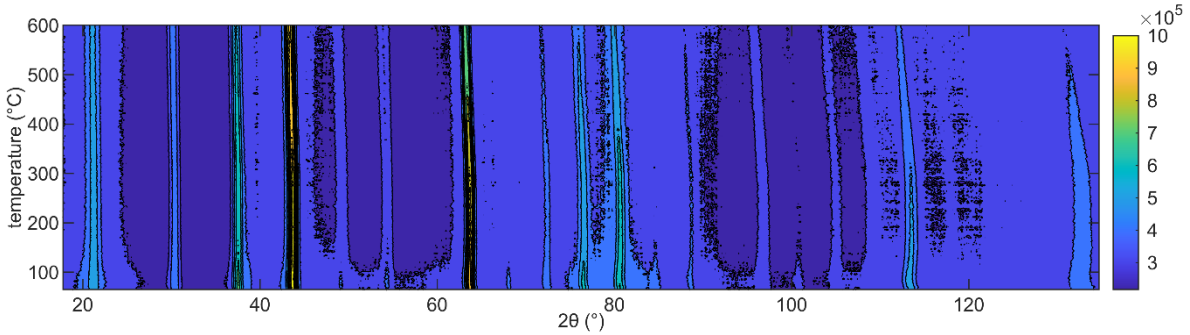

Supplementary Figure 3 Contour plot of NPD for BCFZY between 100 and 600 °C in dry air

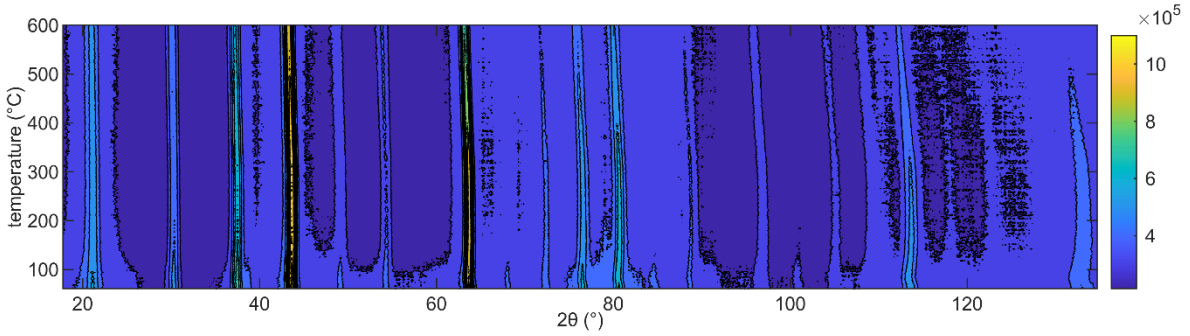

Supplementary Figure 4 Contour plot of NPD for BCFZYYb between 100 and 600 °C in dry air

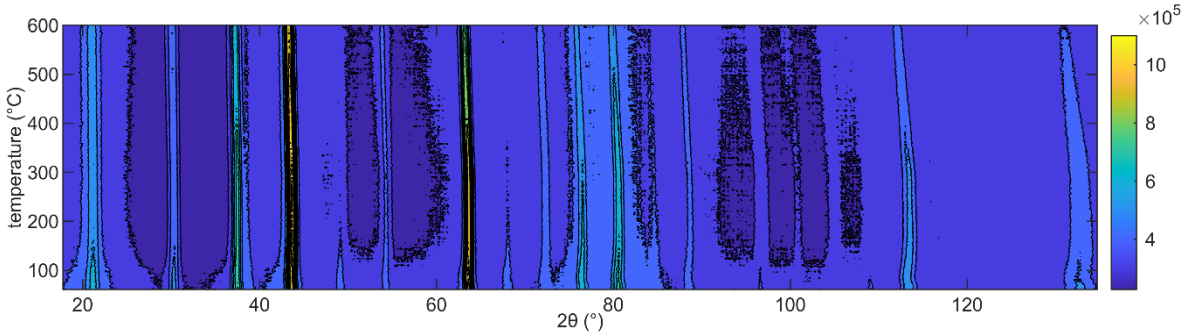

Supplementary Figure 5 Contour plot of NPD for BCFZY between 100 and 600 °C in 3 vol.% D_2O-air

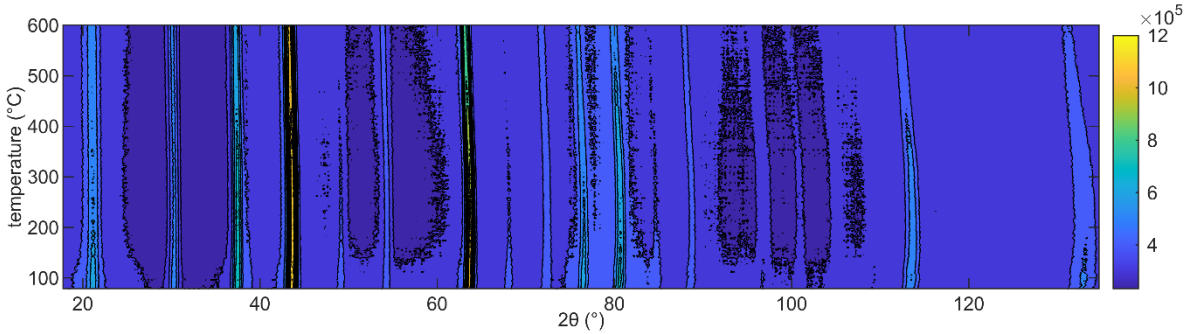

Supplementary Figure 6 Contour plot of NPD for BCFZYYb between 100 and 600 °C in 3 vol.% D_2O-air

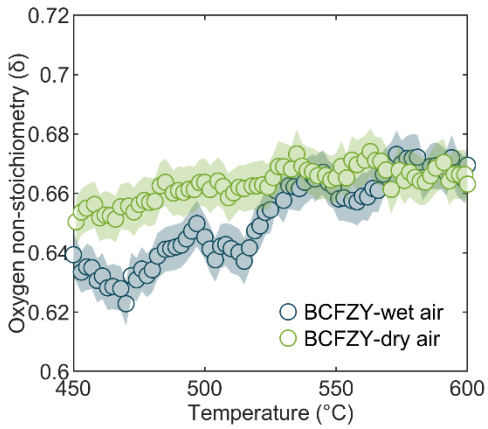

Supplementary Figure 7 Oxygen non-stoichiometry of BCFZY in dry and humid air

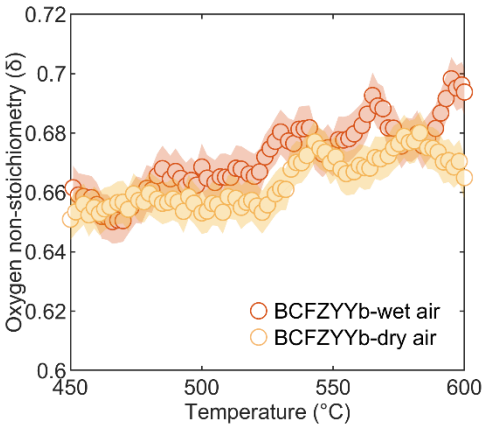

Supplementary Figure 8 Oxygen non-stoichiometry of BCFZYYb in dry and humid air

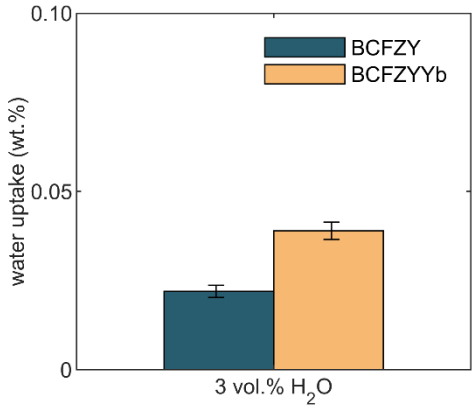

Supplementary Figure 9 Water uptake of BCFZY and BCFZYYb at 400 °C in humid N_2

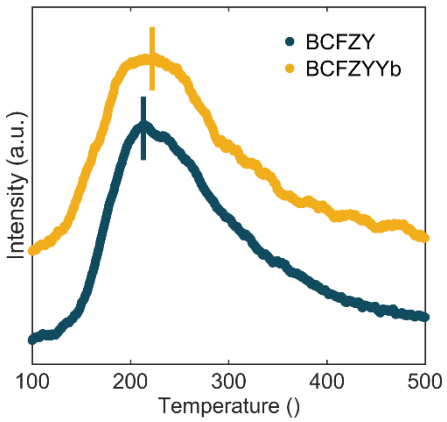

Supplementary Figure 10 H_2O-TPD-MS profile of BCFZY and BCFZYYb

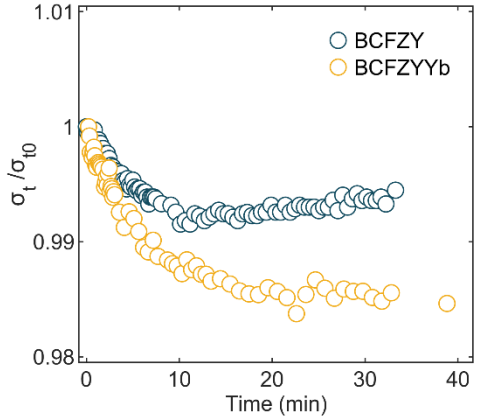

Supplementary Figure 11 ECR of BCFZY and BCFZYYb upon switching from dry to humid air at 500 °C

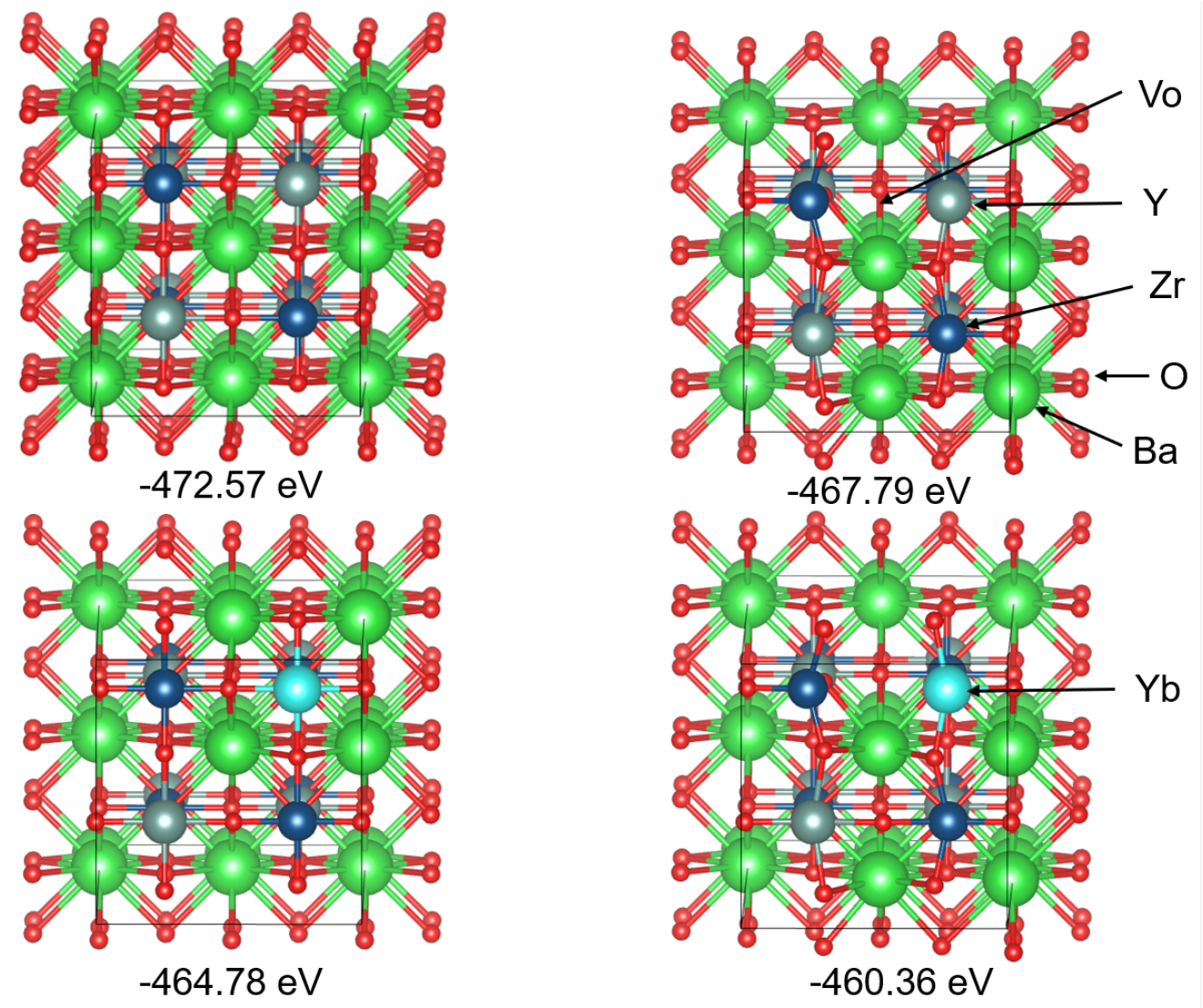

Supplementary Figure 12 DFT modelling results of Ba(Zr, Y)$O_{3-\delta}$ and Ba(Zr, Y, Yb)$O_{3-\delta}$

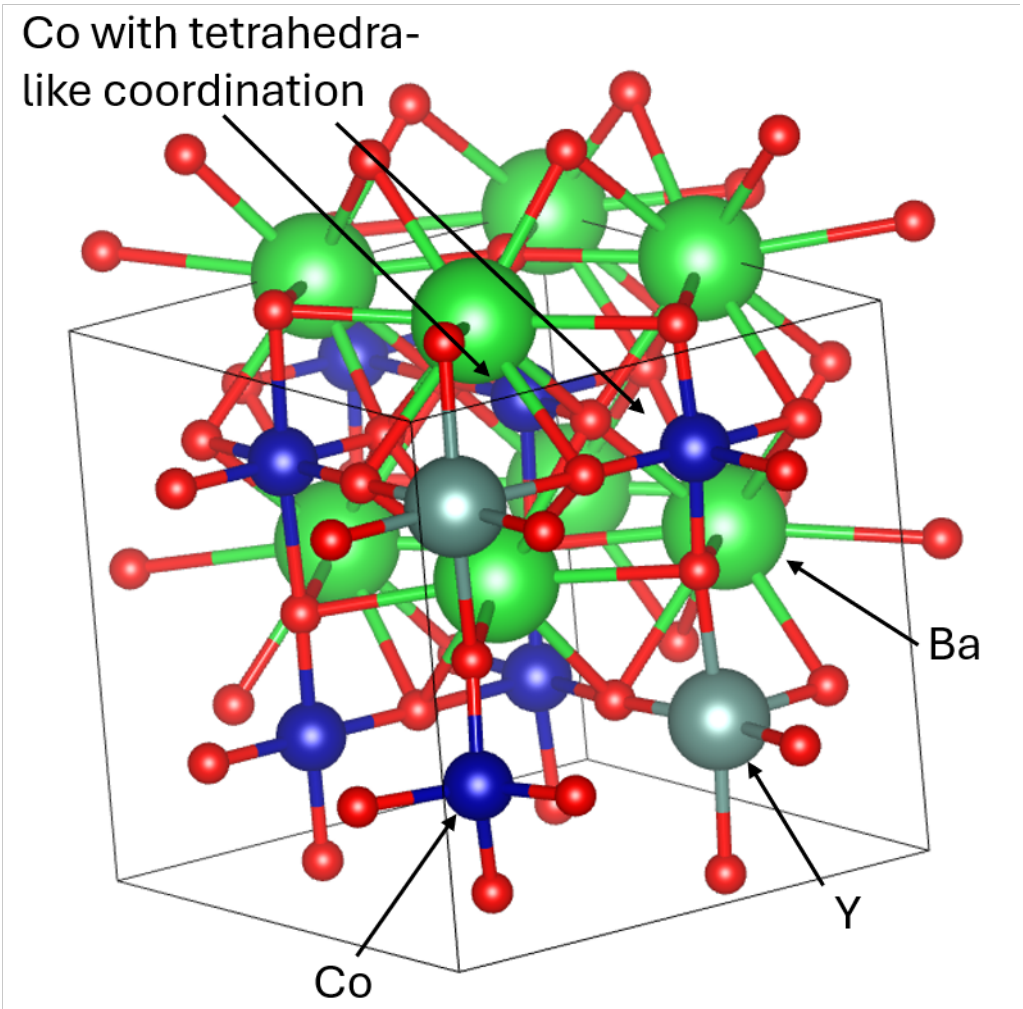

Supplementary Figure 13 DFT modelling results of Ba(Co, Y)$O_{3-\delta}$ with two Yb-Vo-Co-Vo-Co structure

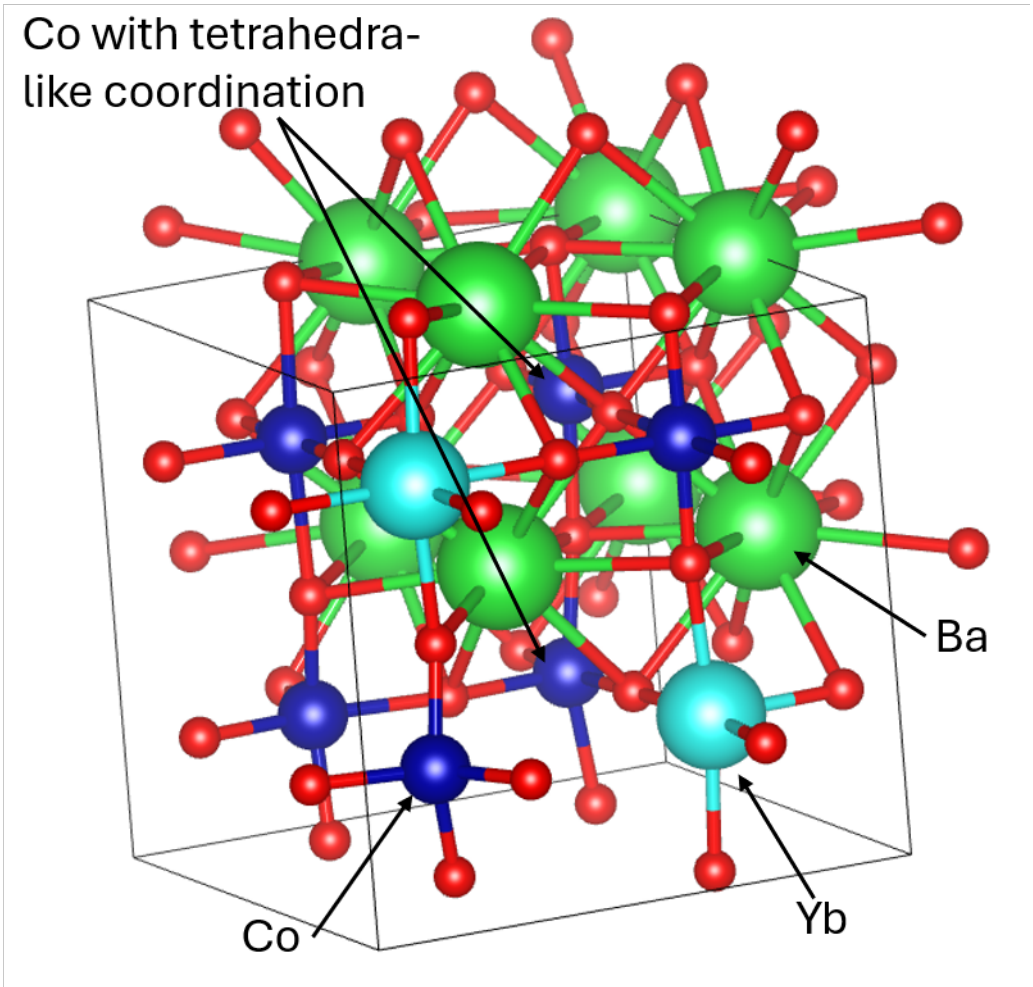

Supplementary Figure 14 DFT modelling results of Ba(Co, Yb)$O_{3-\delta}$ with two Yb-Vo-Co-Vo-Co structure

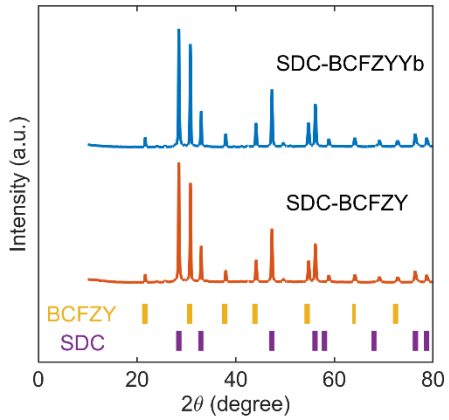

Supplementary Figure 15 XRD pattern of BCFZY/BCFZYYb and SDC mixture after sintering, y-axis is offset for clarity

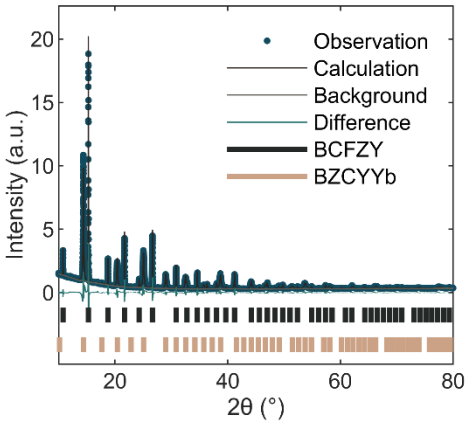

Supplementary Figure 16 SXRD refinement results of BCFZY and BZCYYb mixture after sintering

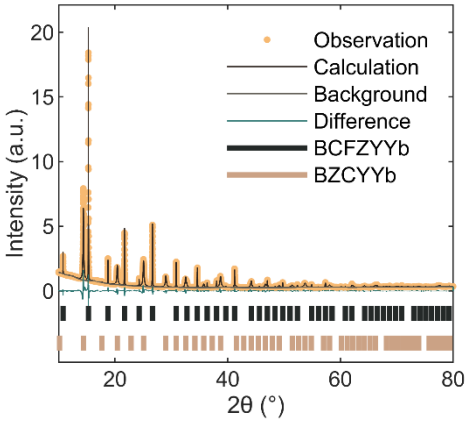

Supplementary Figure 17 SXRD refinement results of BCFZYYb and BZCYYb mixture after sintering

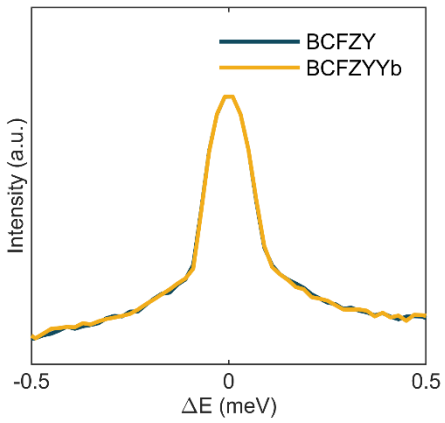

Supplementary Figure 18 QENS results of BCFZY and BCFZYYb at 700 °C

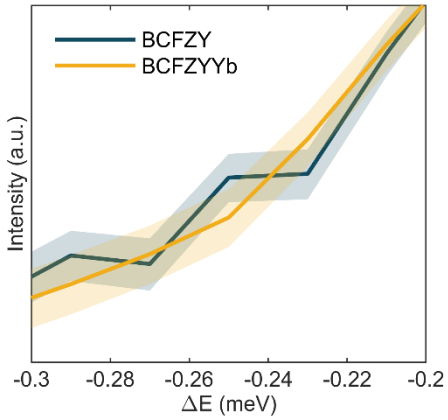

Supplementary Figure 19 Zoom in QENS results of BCFZY and BCFZYYb at 700 °C

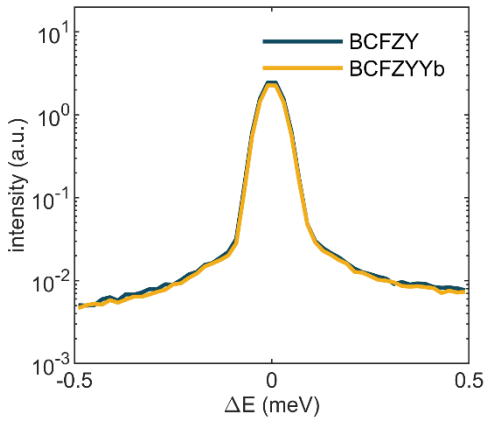

Supplementary Figure 20 QENS results of BCFZY and BCFZYYb at 600 °C

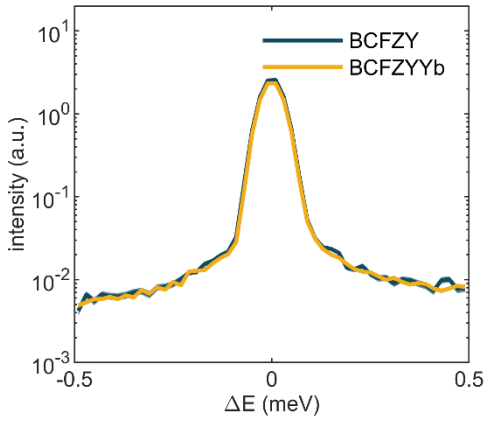

Supplementary Figure 21 QENS results of BCFZY and BCFZYYb at 500 °C

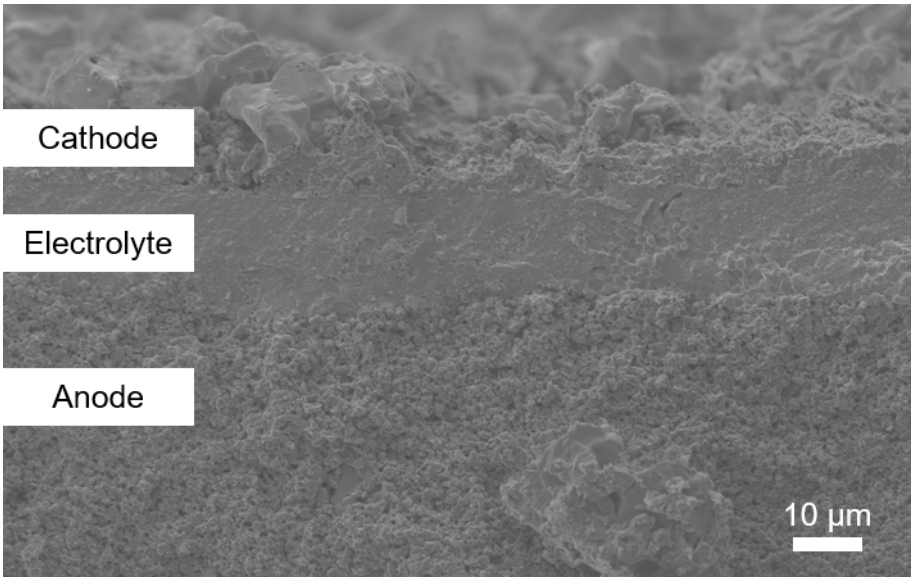

Supplementary Figure 22 Post-mortem SEM image of a single cell containing BCFZYYb cathode

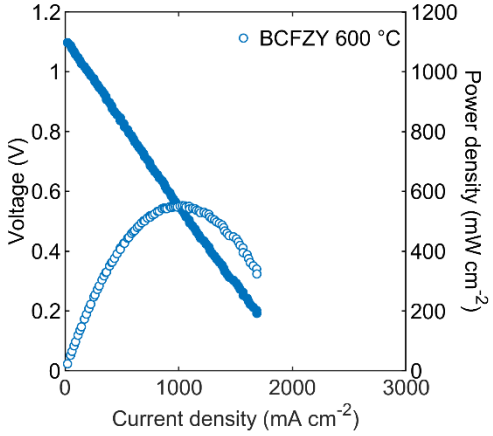

Supplementary Figure 23 Polarisation curve of a single cell containing a BCFZY cathode in humid air

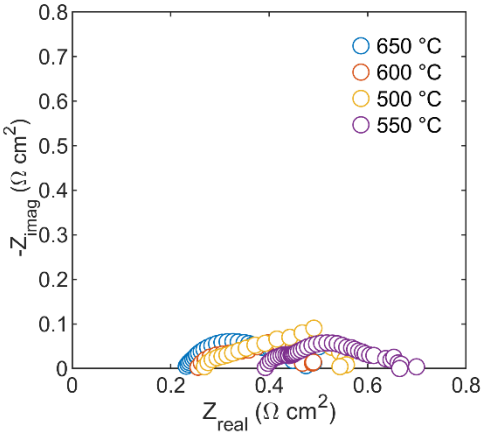

Supplementary Figure 24 EIS results of the single cell containing the BCFZYYb cathode under OCV conditions in humid air

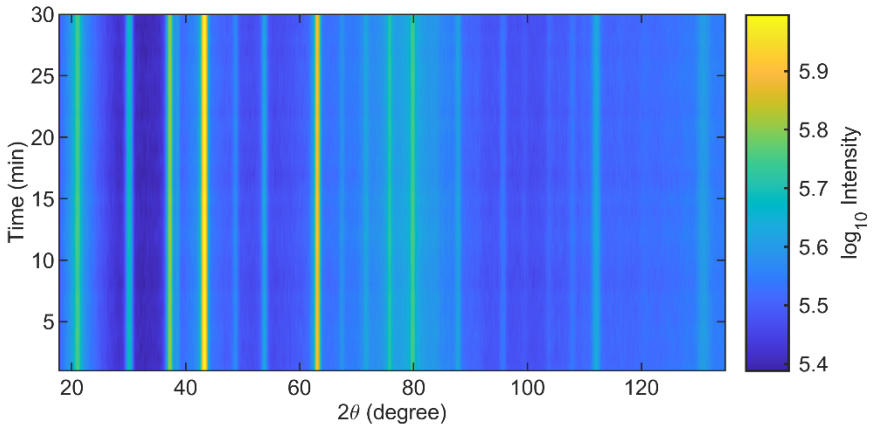

Supplementary Figure 25 NPD contour plot of BCFZY at 600 °C for 2 h

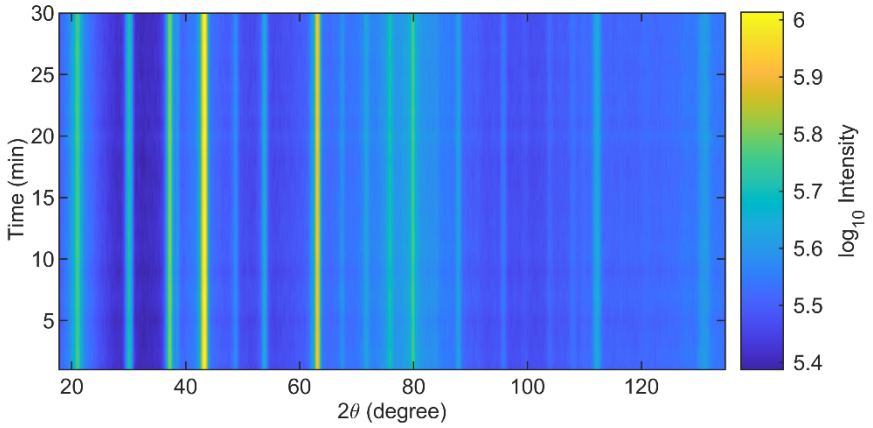

Supplementary Figure 26 NPD contour plot of BCFZYYb at 600 °C for 2 h

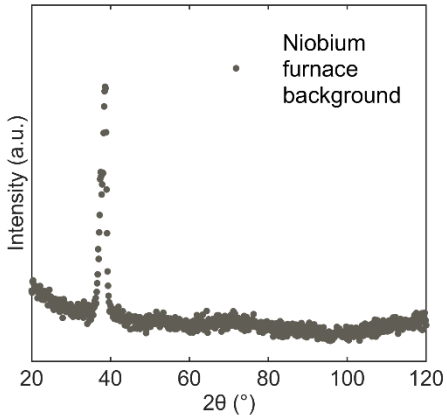

Supplementary Figure 27 The contribution of the vacuum furnace to the NPD pattern

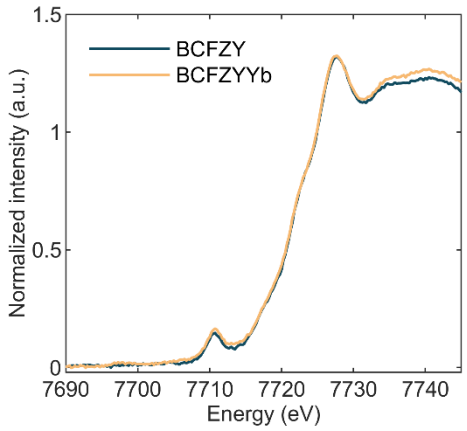

Supplementary Figure 28 Co XAS of BCFZY and BCFZYYb

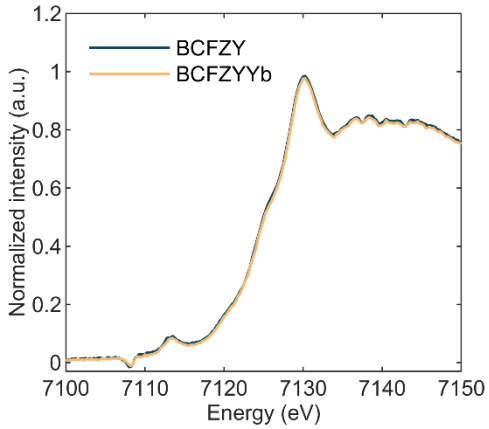

Supplementary Figure 29 Fe XAS of BCFZY and BCFZYYb

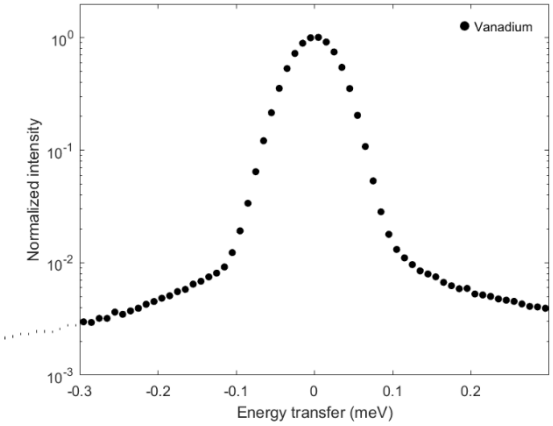

Supplementary Figure 30 Resolution function of Pelican

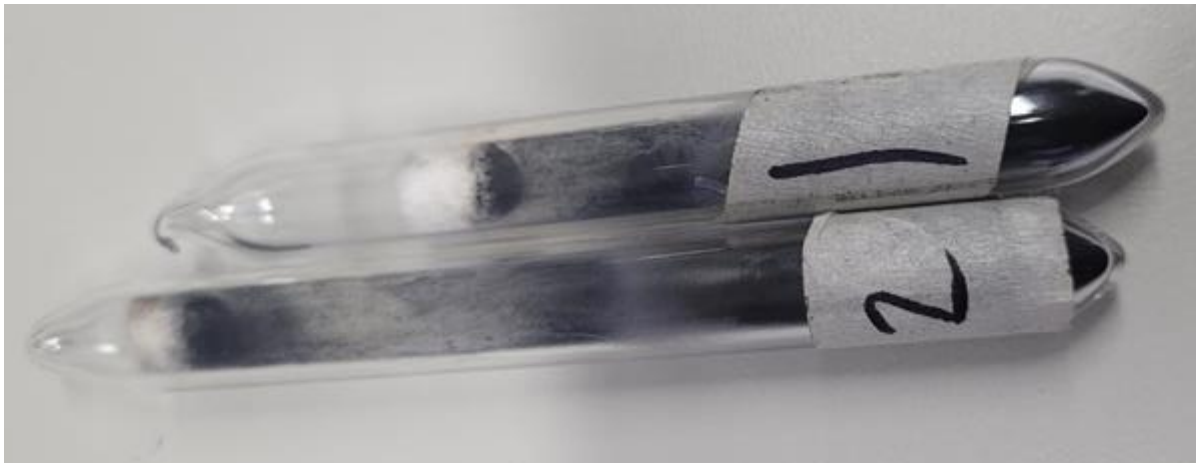

Supplementary Figure 31 A photo of samples in close ampoules for QENS measurement

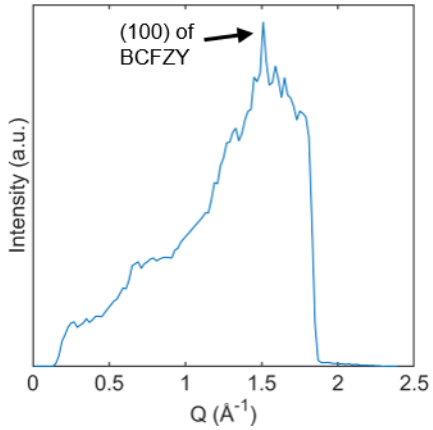

Supplementary Figure 32 S(Q) profile of BCFZY

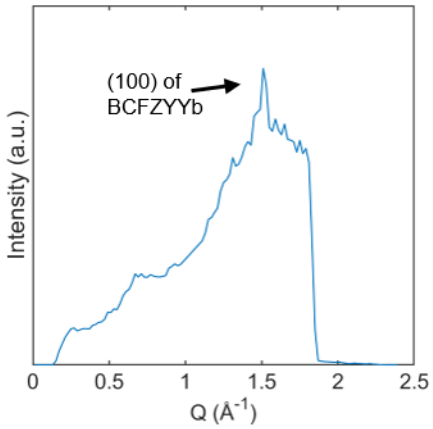

Supplementary Figure 33 S(Q) profile of BCFZYYb

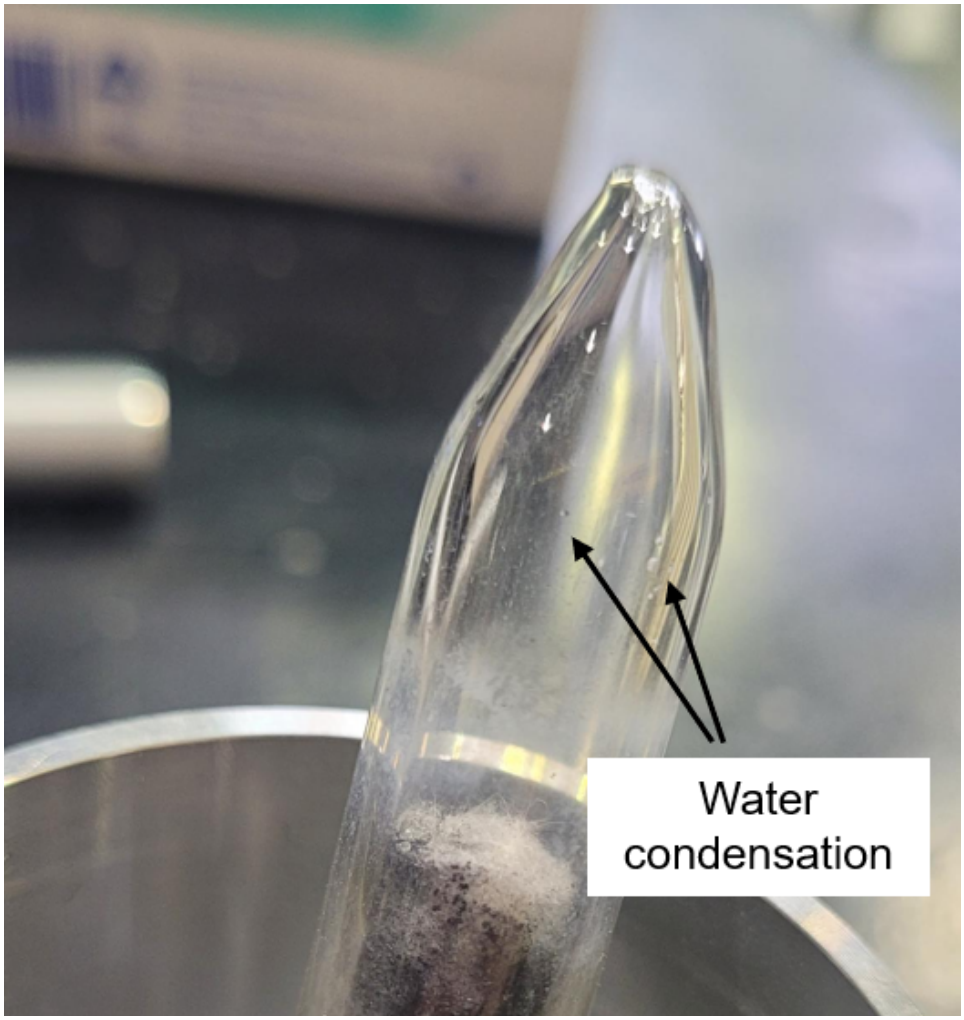

Supplementary Figure 34 A photo of water condensation at the ampoule wall after QENS measurement

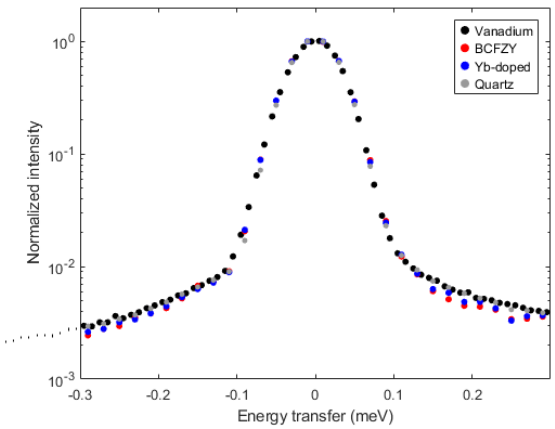

Supplementary Figure 35 Normalised S(E) profiles of BCFZY, BCFZYYb, vanadium and an empty quartz ampoule at 700 °C

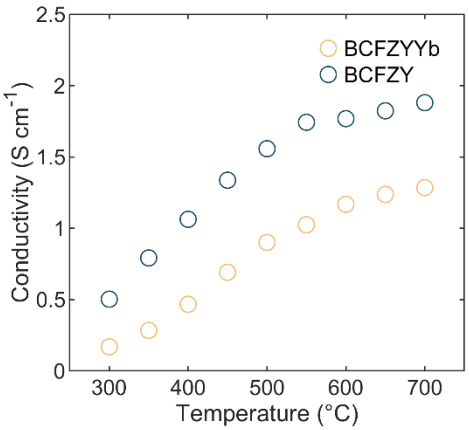

Supplementary Figure 36 electrical conductivity of BCFZY and BCFZYYb measured in dry air between 300 and 700 °C

References

1. Cline, J. P. *et al.* The certification of SRM 640c; the primary NIST line position SRM for powder diffraction. in *The 11th National School and Conference of the Australian X-ray Analytical Association on Analytical X-ray for Industry and Science* 4–4 (1999).
2. Toby, B. H. & Von Dreele, R. B. GSAS-II: the genesis of a modern open-source all purpose crystallography software package. *Journal of Applied Crystallography* **46**, 544–549 (2013).
3. Maynard-Casely, H. E. *et al.* Wombat, the high-intensity diffractometer in operation at the Australian Centre for Neutron Scattering. *J Appl Cryst* **59**, 1–11 (2026).
4. Black, D. R., Windover, D. A., Henins, A., Filliben, J. J. & Cline, J. P. Certification of Standard Reference Material 660b. *Powder Diffraction* https://www.nist.gov/publications/certification-standard-reference-material-660b (2011).
5. Villars, P. & Cenzual, K. BaZr1-xFexO3, x= 0.50 (BaZr0.5Fe0.5O3) Crystal Structure: Datasheet from 'PAULING FILE Multinaries Edition – 2022' in SpringerMaterials (https://materials.springer.com/isp/crystallographic/docs/sd_1244272). Springer-Verlag Berlin Heidelberg & Material Phases Data System (MPDS), Switzerland & National Institute for Materials Science (NIMS), Japan.

6. Sears, V. F. Neutron scattering lengths and cross sections. *Neutron News* **3**, 26–37 (1992).
7. Kresse, G. & Furthmüller, J. Efficiency of ab-initio total energy calculations for metals and semiconductors using a plane-wave basis set. *Computational Materials Science* **6**, 15–50 (1996).
8. Blöchl, P. E. Projector augmented-wave method. *Phys. Rev. B* **50**, 17953–17979 (1994).
9. Ernzerhof, M. & Scuseria, G. E. Assessment of the Perdew–Burke–Ernzerhof exchange-correlation functional. *J. Chem. Phys.* **110**, 5029–5036 (1999).
10. Xiao, W., Yoo, K., Kim, J. & Xu, H. Balanced d-Band Model: A Framework for Balancing Redox Reactions in Lithium–Sulfur Batteries. *ACS Nano* **18**, 32732–32745 (2024).
11. Xiao, W., Yoo, K., Kim, J.-H. & Xu, H. Decoupling Redox Kinetics with Complementary d-Band Catalysis for High-Performance Lithium–Sulfur Batteries. *ACS Nano* **19**, 23223–23234 (2025).
12. Xu, H. Electronegativity-Induced Jahn–Teller Distortion Boosts Li–S Conversion on Asymmetric Cu Single-Atom Catalysts. *J. Phys. Chem. A* **129**, 8744–8750 (2025).
13. Xu, H. & Yu, Z.-W. Biomimetic Geminal-Atom Catalysts Empowered by Jahn–Teller Distortion: A Theoretical Study for Efficient PET Degradation. *J. Phys. Chem. Lett.* **16**, 6787–6793 (2025).
14. Xiao, W., Yoo, K., Kim, J.-H. & Xu, H. Breaking Barriers to High-Practical Li-S Batteries with Isotropic Binary Sulfiphilic Electrocatalyst: Creating a Virtuous Cycle for Favorable Polysulfides Redox Environments. *Advanced Science* **10**, 2303916 (2023).
15. Xu, H. Bio-Inspired Curvature Engineering across the Periodic Table Tunes Hydrogen Adsorption in Single-Atom Catalysts. *J. Phys. Chem. Lett.* **17**, 665–671 (2026).
16. Xu, H. Atomic-scale insights into the electrochemical mechanisms of aluminum-sulfur batteries: A first-principles study of Al-S clusters on graphene. *Chemical Physics Letters* **851**, 141492 (2024).

17. Sun, Y. *et al.* Covalency competition dominates the water oxidation structure–activity relationship on spinel oxides. *Nat Catal* **3**, 554–563 (2020).
18. Zhang, H. *et al.* Self-Optimized Interfacial Co–O–Ru Motifs of Hollow Nanotube Composites Trigger Interfacial Lattice Oxygen Participation and Diffusion. *ACS Nano* **19**, 25917–25929 (2025).
19. Yu, D., Mole, R. A. & Kearley, G. J. Performance test on PELICAN – a multi-purpose time of flight cold neutron spectrometer. *EPJ Web of Conferences* **83**, 03019 (2015).
20. Yu, D., Mole, R., Noakes, T., Kennedy, S. & Robinson, R. Pelican — a Time of Flight Cold Neutron Polarization Analysis Spectrometer at OPAL. *J. Phys. Soc. Jpn.* **82**, SA027 (2013).
21. Wang, Z. *et al.* Rational design of perovskite ferrites as high-performance proton-conducting fuel cell cathodes. *Nat Catal* **5**, 777–787 (2022).
22. Saqib, M. *et al.* Transition from perovskite to misfit-layered structure materials: a highly oxygen deficient and stable oxygen electrode catalyst. *Energy Environ. Sci.* **14**, 2472–2484 (2021).
23. Liang, M. *et al.* Nickel-doped BaCo0.4Fe0.4Zr0.1Y0.1O3-δ as a new high-performance cathode for both oxygen-ion and proton conducting fuel cells. *Chemical Engineering Journal* **420**, 127717 (2021).
24. Song, R. *et al.* A novel triple-conductive cathode with high efficiency and stability for protonic ceramic fuel cells. *International Journal of Hydrogen Energy* **48**, 32943–32954 (2023).
25. Liang, M. *et al.* Magnesium tuned triple conductivity and bifunctionality of BaCo0.4Fe0.4Zr0.1Y0.1O3-δ perovskite towards reversible protonic ceramic electrochemical cells. *Applied Catalysis B: Environmental* **318**, 121868 (2022).
26. Kim, J. H. *et al.* An universal oxygen electrode for reversible solid oxide electrochemical cells at reduced temperatures. *Energy Environ. Sci.* **16**, 3803–3814 (2023).

27. Shin, Y. *et al.* Tuning the Co/Fe ratio in BaCoxFe0.8−xZr0.1Y0.1O3−δ, a promising triple ionic and electronic conducting oxide, to boost electrolysis and fuel cell performance. *J. Mater. Chem. A* **10**, 24839–24853 (2022).
28. Wang, X. *et al.* Highly ionic-dispersed oxygen electrode for reversible proton ceramic electrochemical cells. *Nat Commun* **17**, 3989 (2026).
29. Zhao, S. *et al.* Reverse Atom Capture on Perovskite Surface Enabling Robust and Efficient Cathode for Protonic Ceramic Fuel Cells. *Advanced Materials* **36**, 2405052 (2024).